Roles of linear and circular polarization properties and effect of wavelength choice on differentiation between *ex vivo* normal and cancerous gastric samples

Wenfeng Wang
Lee Guan Lim
Supriya Srivastava
Jimmy So Bok Yan
Asim Shabbir
Quan Liu

SPIE

Roles of linear and circular polarization properties and effect of wavelength choice on differentiation between *ex vivo* normal and cancerous gastric samples

Wenfeng Wang,[a] Lee Guan Lim,[b] Supriya Srivastava,[c] Jimmy So Bok Yan,[d] Asim Shabbir,[c] and Quan Liu[a],*
[a]Nanyang Technological University, School of Chemical and Biomedical Engineering, Nanyang Avenue, Singapore 637457, Singapore
[b]National University Health System, Division of Gastroenterology and Hepatology, Kent Ridge Road, Singapore 119228, Singapore
[c]National University of Singapore, Cancer Science Institute, Lower Kent Ridge Road, Singapore 117599, Singapore
[d]National University of Singapore, Department of Surgery, Lower Kent Ridge Road, Singapore 119228, Singapore

Abstract. Multispectral Mueller matrix imaging was performed over a spectral range from 470 to 632 nm on 4-μm unstained gastric tissue sections. A complete set of polarization parameters was derived. The combination of linear depolarization and linear retardance yields the highest accuracy in sample classification. When the depolarization of linearly polarized light due to scattering is independent of the orientation angle of the incident linear polarization vector, the derivation of linear polarization properties will require only 3×3 Mueller matrix, which would significantly reduce the complexity of the polarimetry imaging system. When additional parameters are needed to complement the two linear polarization parameters, retardance, circular depolarization, and depolarization can be included in classification in the order of preference. However, these additional parameters would require the measurement of 4×4 Mueller matrix. In addition, it appears that wavelength is not a critical factor in terms of classification accuracy for thin tissue sections in this study. © *2014 Society of Photo-Optical Instrumentation Engineers (SPIE)* [DOI: 10.1117/1.JBO.19.4.046020]

Keywords: polarimetry imaging; spectral imaging; Mueller matrix; transmission measurements; tissue sections.

Paper 130873RR received Dec. 8, 2013; revised manuscript received Mar. 25, 2014; accepted for publication Mar. 31, 2014; published online Apr. 28, 2014.

1 Introduction

Several morphological changes, which include enlarged nuclei and cell size and changes in nuclei density and cell distribution,[1] can occur when biological tissues develop into cancer. These changes are reflected in tissue polarization properties which can be measured by polarimetry techniques.[2] Specifically, polarization properties, such as retardance, depolarization, and diattenuation, can be derived by performing polar decomposition of the Mueller matrices measured from tissues.[3,4] It is worth noting that Swami et al[5] proposed that linear polarization properties, including linear polarization, linear retardance, and linear diattenuation, as well as circular retardance, can be reconstructed from 3×3 Mueller matrix, which corresponds to the first nine elements of 4×4 full Mueller matrix, under the assumption that the depolarization of linearly polarized light due to scattering is independent of the orientation angle of the incident linear polarization vector. However, other circular polarization properties, such as circular depolarization and circular diattenuation, cannot be derived. Compared to other optical techniques based on different contrasts, such as fluorescence spectroscopy and imaging,[6–8] polarimetry imaging has great advantages in signal strength and sensitivity to cellular structures. While the former advantage enables fast data acquisition, the latter one facilitates the characterization of structural changes in tissues.

Differences in polarization parameters have been frequently observed between malignant and normal tissues. Smith et al.[9] characterized various dermatological diseases using Mueller matrix polarimetry imaging. Their preliminary results at 633 nm showed that both lupus lesions and malignant moles could be identified by polarimetric measurement. Baldwin et al.[10] suggested that normal, benign moles and cancerous lesions could be potentially differentiated by multiple Mueller matrix elements. Chung et al.[4] used a high-speed polarimetry system to image oral precancer on hamster cheek pouches and observed considerable differences in depolarization images and retardance images between normal and precancerous tissues. Similarly, it was found by Shukla et al.[11] that depolarization power was sensitive to morphological changes from normal to dysplastic state in epithelial cervical tissue, while changes in stromal region were revealed in retardance values. Due to the potential of polarimetry imaging in cancer diagnosis, various approaches have been proposed to acquire data rapidly and derive polarimetry parameters. Manhas et al.[12] developed a system to obtain 3×3 Mueller matrix and demonstrated that the values of all linear polarization parameters, i.e., linear retardance, linear depolarization (LD), and linear diattenuation, in normal oral cavity tissues were higher than cancerous tissues at wavelengths ranging from 400 to 550 nm. This observation was the opposite of that in breast tissues based on their results. Pierangelo et al.[13] observed enhanced contrasts for staging human colon and distinguishing between various histological

variants of tumor by looking at depolarization and M22 from multispectral Mueller matrices. Laude-Boulesteix et al.[14] built a Mueller polarimetric imaging system with liquid crystals and observed differences in polarization properties including retardance, diattenuation, and depolarization among different wavelengths in a hepatic tissue sample. Soni et al.[15] built a spectral Mueller matrix polarimetric system for both fluorescence and elastic scattering measurements recently, in which strong diattenuation was observed in the connective region of a tissue sample from cervical precancer. Despite a large number of publications in this field, none of the above reports about polarimetry imaging have compared the potential of circular polarization properties, including circular retardance and circular depolarization, with that of linear polarization properties to find out whether it is necessary to acquire 4×4 Mueller matrix instead of 3×3 Mueller matrix that can only be used to extract linear properties or an even smaller matrix at multiple wavelengths. Since adding circular polarization into a Mueller matrix imaging system could induce significant complexity and cost, the question is worth systematic investigation. Moreover, the influence of light wavelength choice on optical diagnosis in polarimetry imaging has not been studied systematically for gastric tissues.

In this paper, we investigate the relative importance of both linear and circular polarization parameters, derived from 4×4 Mueller matrix measurements, in discriminating cancer from normal gastric tissues over the visible spectral region from 470 to 632 nm. Moreover, the diagnostic value of each wavelength is compared against each other. Our results answer the questions proposed in the previous paragraph, which will guide the design of a portable polarimetry imaging system for *in vivo* examination of gastric tissues. It should be noted that the novelty of this paper is not about the development of a multispectral polarimetry imaging system, but rather the investigation on the importance of linear and circular polarization parameters and wavelength choices using the imaging system.

2 Methods

2.1 Decomposition of Mueller Matrix

The Mueller matrix of a depolarizing sample can be expressed as the product of three 4×4 matrices: the depolarization matrix (M_Δ), the retardance matrix (M_R), and the diattenuation matrix (M_d). The procedure is briefly described below:[4,16,17]

The Mueller matrix (M) is decomposed in the following order using the polar decomposition method,[16] which has been used as a robust mathematical tool to interpret the polarization properties of a medium as illustrated and applied in several other papers[4,11,13,17]

$$M = \begin{bmatrix} m_{00} & m_{01} & m_{02} & m_{03} \\ m_{10} & m_{11} & m_{12} & m_{13} \\ m_{20} & m_{21} & m_{22} & m_{23} \\ m_{30} & m_{31} & m_{32} & m_{33} \end{bmatrix}, \quad (1)$$

$$M = M_\Delta \times M_R \times M_d. \quad (2)$$

The diattenuation (D) value is derived from the elements on the first row of the matrix using the following equation:[16]

$$D = \frac{1}{m_{00}} \sqrt{m_{01}^2 + m_{02}^2 + m_{03}^2}. \quad (3)$$

Then, the diattenuation property is removed by multiplying Mueller matrix (M) by the inversion of diattenuation matrix (M_d) to get M'[16]

$$M' = M_\Delta M_R = M M_d^{-1}. \quad (4)$$

These above matrices have the following forms:[16]

$$M_\Delta = \begin{bmatrix} 1 & \vec{0}^T \\ \vec{P}_\Delta & m_\Delta \end{bmatrix} M_R = \begin{bmatrix} 1 & \vec{0}^T \\ \vec{0} & m_R \end{bmatrix} M' = \begin{bmatrix} 1 & 0^T \\ \vec{P}_\Delta & m' \end{bmatrix}, \quad (5)$$

where, m_Δ, m_R, and m' are the 3×3 submatrices of M_Δ, M_R, and M', respectively. $m' = m_\Delta \times m_R$ and m_Δ can be computed as[16]

$$m_\Delta = \pm [m'(m')^T + (\sqrt{\lambda_1 \lambda_2} + \sqrt{\lambda_2 \lambda_3} + \sqrt{\lambda_3 \lambda_1})I]^{-1} \\ \times [(\sqrt{\lambda_1} + \sqrt{\lambda_2} + \sqrt{\lambda_3})m'(m')^T + \sqrt{\lambda_1 \lambda_2 \lambda_3}I], \quad (6)$$

where λ_1, λ_2, and λ_3 are the eigenvalues of $m'(m')^T$. Noted that if the determinant of m' is positive, we choose the positive sign on the right side of the above equation; otherwise, the negative sign is used. Further, the depolarization power (Δ) and the submatrix of retardance matrix (m_R) can be calculated[16]

$$\Delta = 1 - \frac{|\text{trace}(m_\Delta)|}{3}, \quad (7)$$

$$m_R = m_\Delta^{-1} m'. \quad (8)$$

This enables one to calculate the retardance matrix M_R according to Eq. (5).

Finally, the retardance (R), linear retardance (δ), and circular retardance (φ) are calculated as follows:[5,17,18]

$$R = \cos^{-1} \left[\frac{\text{trace}(M_R)}{2} \right] - 1 \quad (9)$$

$$\delta = \cos^{-1} \left(\left\{ \begin{array}{l} [M_R(2,2) + M_R(3,3)]^2 \\ + [M_R(2,3) - M_R(3,2)]^2 \end{array} \right\}^{1/2} - 1 \right), \quad (10)$$

$$\varphi = \frac{1}{2} \tan^{-1} \left[\frac{M_R(2,3) - M_R(3,2)}{M_R(2,2) + M_R(3,3)} \right]. \quad (11)$$

According to the original Mueller matrix M, the linear degree of polarization (LDOP) and circular degree of polarization (CDOP) are obtained as[19]

$$\text{LDOP} = \frac{m_{10} + m_{11}}{m_{00} + m_{01}}, \quad (12)$$

$$\text{CDOP} = \frac{m_{30} + m_{33}}{m_{00} + m_{03}}, \quad (13)$$

in which LDOP describes to what degree the linearly polarized light preserves its polarization state after interaction with sample, whereas CDOP denotes to what degree the circular

polarization of light is preserved. Then, linear depolarization (LD) and circular depolarization (CD) can be computed as

$$LD = 1 - LDOP, \tag{14}$$

$$CD = 1 - CDOP. \tag{15}$$

2.2 Materials and Instruments

A total of 46 tissue samples, obtained from 40 patients, were examined in this study, in which 26 normal gastric samples were obtained as endoscopic biopsies, whereas 20 gastric cancer samples were from gastrectomy. All patients had to sign a written consent form before their tissue samples were used in this study. For multiple normal samples from one single patient, the values of polarization parameters were averaged to represent only one sample in classification. This procedure yielded a total of 20 sets of data for normal samples and 20 sets of data for cancer samples, one set for each patient. Each sample was fixed using 10% formalin solution before it was embedded in paraffin. Then, two 4-μm vertical sections immediately next to each other were made in the sample. One tissue section was routinely stained with hematoxylin and eosin (H&E) to generate a pathological report. The other tissue section was not stained and was placed on a microscope slide without a cover slip for polarimetry measurements.

The schematic of the multispectral Mueller matrix polarimetry system used in this study is shown in Fig. 1, in which all optical components are mounted in a commercial microscope (Ti-U, Nikon, Tokyo, Japan). The illumination light from a 100-W-halogen lamp is polarized by a polarization state generator (PSG) that consists of a linear polarizer (Model No. 47213, Edmund Optics, Barrington, New Jersey, US), mounted in a filter wheel (HF110, Prior Scientific Instrument, Fulbourn, Cambridge, UK), followed by a nematic liquid crystal variable retarder (LCVR) (LCVR-1-VIS, Thorlabs, Newton, New Jersey, US). After passing through the sample, the transmitted light is analyzed by a polarization state analyzer (PSA) with the same optical components but in reverse order. The Mueller matrix images are recorded on a charged coupled device (DS-Qi1Mc, Nikon, Tokyo, Japan) with a resolution of 640×512 pixels.

A total of nine bandpass filters with central wavelengths of 470, 488, 508, 532, 550, 568, 589, 610, and 632 nm (Product Nos. 65144, 65147, 65151, 65155, 65159, 65160, 65162, 65164, and 65166, Edmund Optics, Barrington, New Jersey, US) with a bandwidth of around 10 nm were mounted in a filter wheel to enable miltispectral imaging. The light spot focused on the sample is about 3 mm in diameter under 2X objective lens. In most normal samples obtained from biopsy, the entire area of specimens can be covered in the field of view. For each cancer sample obtained from surgery with a larger size, repeated measurements were made at multiple locations and the results were averaged to represent the entire sample, which was to take into account large heterogeneity in cancer samples.

2.3 Imaging Method

Both PSG and PSA can generate the following polarization states by switching between the linear polarizers with different orientations and adjusting the retardance of LCVR, which includes horizontal polarization (stokes vector H:$[1100]^T$), vertical polarization (V:$[1{-}100]^T$), +45 deg linear polarization (P:$[1010]^T$), and right circular polarization (R:$[1001]^T$). Sixteen images corresponding to HH, HV, HP, HR, VH, VV, VP, VR, PH, PV, PP, PR, RH, RV, RP, and RR, in which the two letters indicate the polarization states of the PSG and the PSA respectively, were recorded at nine wavelengths. After background subtraction, the acquired images were used to reconstruct the Mueller matrix,[20] which was then decomposed to extract polarization parameters using polar decomposition.[4]

Each tissue sample was fixed on a microscope slide during measurements. To minimize the uncertainty in the Mueller matrix of a sample due to the microscope slide and the system components, the following calibration was performed for every tissue sample. For each sample fixed on a slide, one blank location of the slide was measured first and the slide's Mueller matrix (M_b) was reconstructed. Then, the sample location on the slide was measured and the Mueller matrix of the sample on top of the slide (M_{b+s}) was reconstructed. Finally, the Mueller matrix of the sample on top of the slide was multiplied by the inversion of the slide's Mueller matrix to yield the true Mueller matrix of the sample (M_s) in which the effects of the slide and system throughput have been removed. Mathematically, this process can be denoted as

$$M_s = M_{b+s} \times M_b^{-1}. \tag{16}$$

We validated the experimental setup (Fig. 1) and the approach of matrix inversion in the previous paragraph by measuring the Mueller matrix of a quarter-wave plate, a half-wave plate, and a linear polarizer with known polarization properties prior to imaging gastric tissue samples. These standard samples were put on top of a microscope slide and the effects of slides were removed after measurements. The results of these measurements are shown at the beginning of the next section, which suggests that the experimental setup works well.

3 Results

The normalized Mueller matrix of a horizontal linear polarizer at different wavelengths and the retardance of a half-wave plate and a quarter-wave plate are shown in Figs. 2(a) and 2(b), respectively. In Fig. 2(a), the differences between experimental measurements and theoretical prediction for the linear polarizer are smaller than 0.06 when all elements are divided by m_{00} at the corresponding wavelength. Similarly, as shown in Fig. 2(b), the measured retardance value differs from the reference value given by the manufacturer by less than 2% for both the half-wave plate and the quarter-wave plate. The small discrepancies could be attributed to the finite bandwidth of the bandpass filter at each wavelength and the slight variation in the retardance of
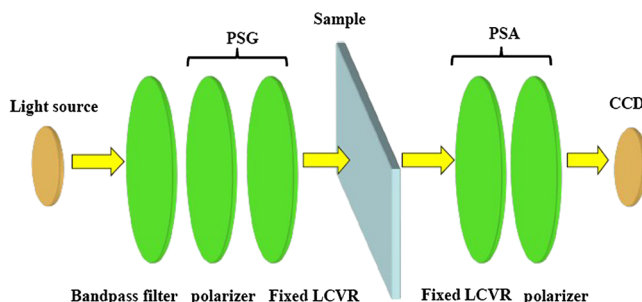

Fig. 1 Schematic of the polarimetry imaging system to record 4×4 Mueller matrix at multiple wavelengths.
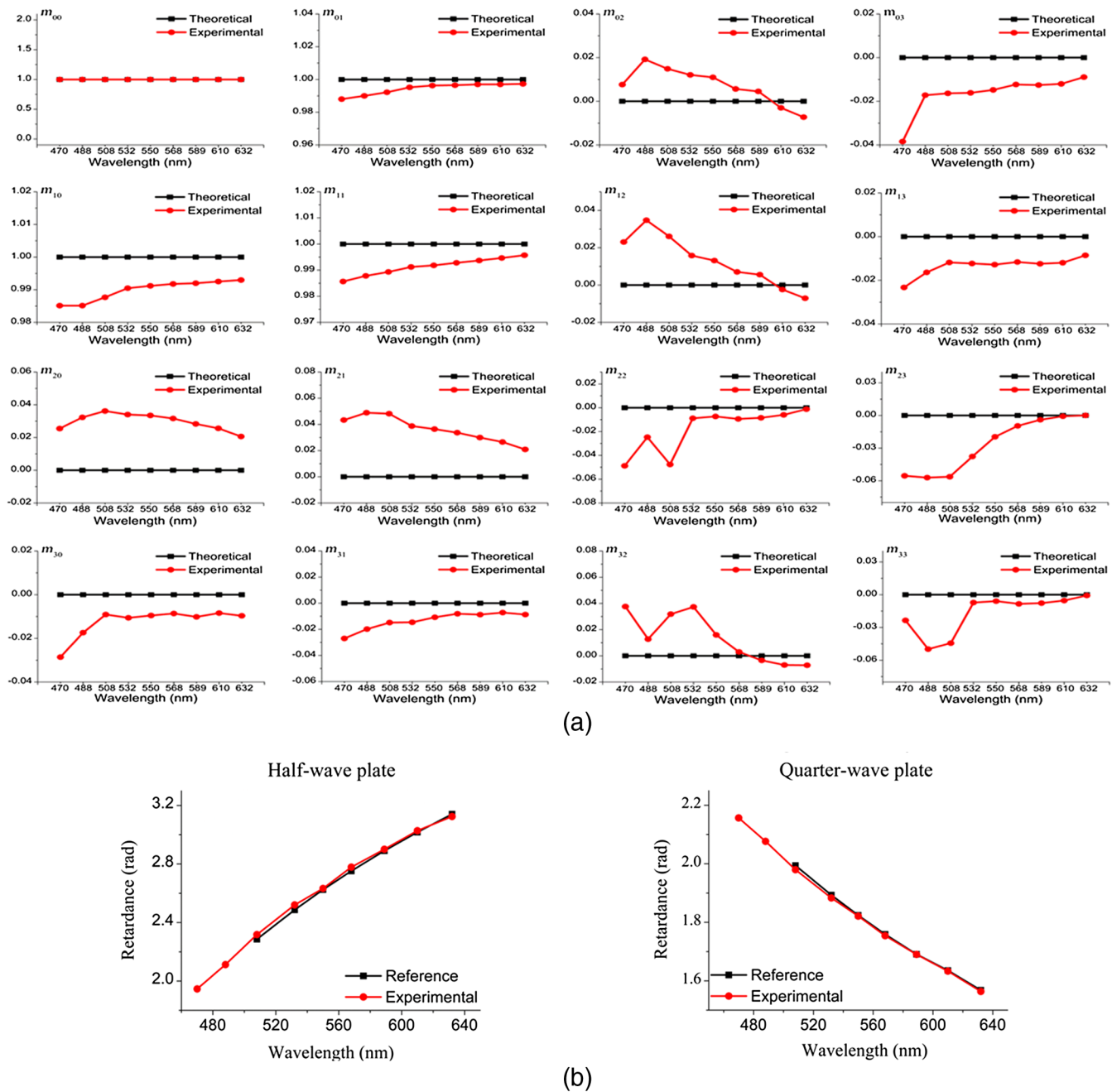
(a)

(b)

Fig. 2 (a) Mueller matrix elements of a horizontal linear polarizer (experimental and theoretical values) and (b) retardance values of a half-wave plate (left) and a quarter-wave plate (right) at nine different wavelengths (experimentally measured values and reference values provided by the manufacturer) ranging from 470 to 632 nm. In Fig. 2(a), the vertical axis represents the value of each Mueller matrix element divided by m_{00}.

the LCVR due to temperature fluctuation. The reference retardance values of two wave plates at 470 and 488 nm are not available from the manufacturer thus not shown in Fig. 2(b). The excellent agreement in the Mueller matrix of the linear polarizer between experimental measurements and theoretical prediction and the agreement in the retardance values of the wave plates between experimental measurements and reference values provided by manufacturers demonstrate that the Mueller matrix imaging system and data analysis methods work well. In addition, the standard deviations of retardance, linear retardance, depolarization, linear depolarization, and circular depolarization

values for gastric samples measured in different days are more than four times larger than those for those standard samples such as air, polarizer, and retarders. In contrast, the standard deviations of diattenuation and circular retardance for the standard samples are only about twice those for gastric samples. This observation suggests that the major portion of the variances in the former five parameter values of tissue samples is contributed by tissue samples while a large portion of the variances in the latter two parameter values of tissue samples is contributed by the system, which will influence data interpretation as discussed later.

Figure 3 shows the following derived polarization parameters, i.e., (a) retardance, (b) diattenuation, and (c) depolarization of normal and cancerous gastric samples at nine wavelengths from 470 to 632 nm. The average retardance of normal samples is smaller than that of cancer samples. There is no overlap in the error bars between normal and cancerous samples at all nine wavelengths, which suggest that retardance could be effectively used to differentiate normal and cancer samples. In contrast, there are significant overlaps in the error bars for diattenuation and visible overlaps in those for depolarization between normal and cancer samples at all wavelengths.

To further identify the contributions from linearly and circularly polarized light, linear and circular retardances are plotted as a function of wavelength as shown in Fig. 4. The linear retardance value is similar to the retardance value at each wavelength, implying that linear retardance is the main contributor of retardance in gastric tissues. Linear retardance also similarly shows a significant difference between normal and cancerous samples. In contrast, circular retardance is much smaller and the overlaps in error bars between normal tissues and cancer are significant, which suggests potentially insignificant diagnostic value. Linear and circular depolarizations are also plotted as a function of wavelength as shown in Fig. 5. The general trend, i.e., the depolarization of normal samples is smaller than that of cancer samples, is consistent for both linear and circular depolarizations. The subtle difference is that the overlaps in the error bars of
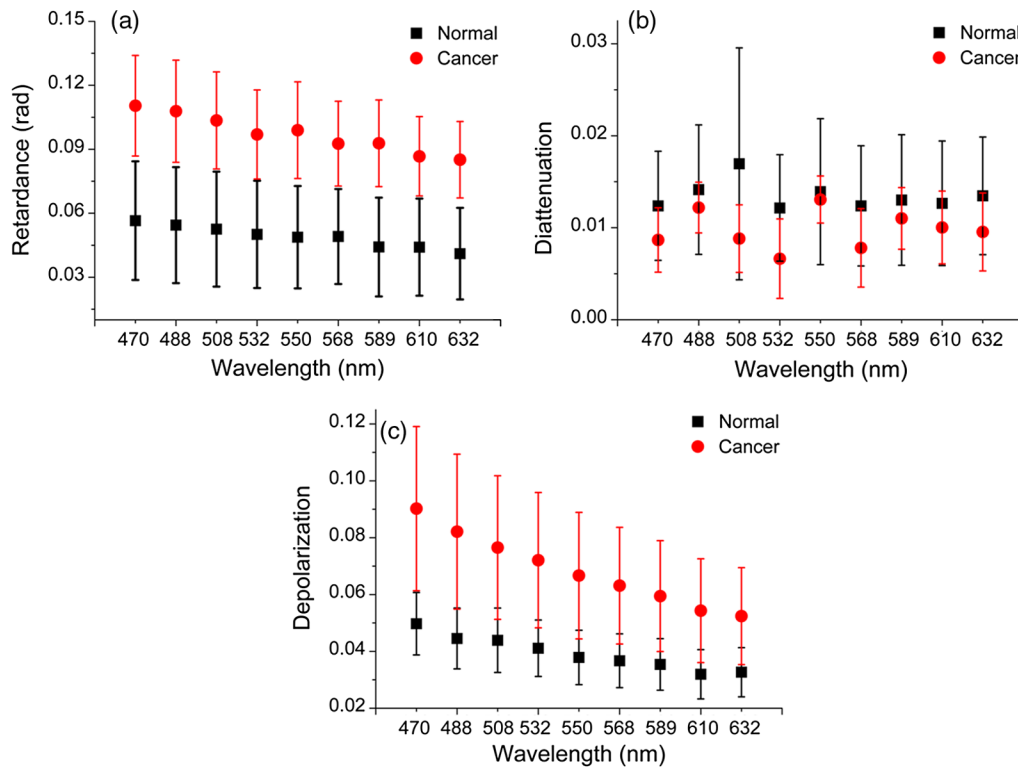

Fig. 3 Polarization parameters including the (a) retardance, (b) diattenuation, and (c) depolarization of normal (■) and cancerous (●) gastric samples at nine different wavelengths ranging from 470 to 632 nm.
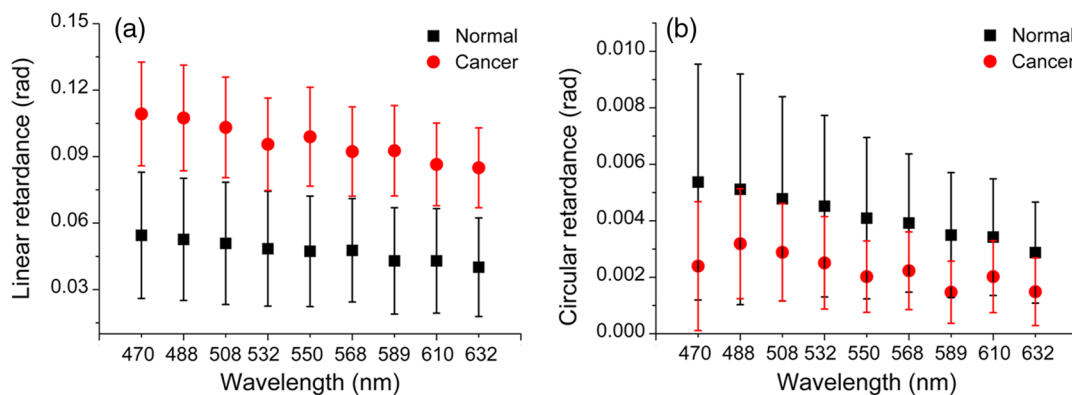

Fig. 4 (a) Linear retardance and (b) circular retardance of normal (■) and cancerous (●) gastric samples at nine different wavelengths ranging from 470 to 632 nm.
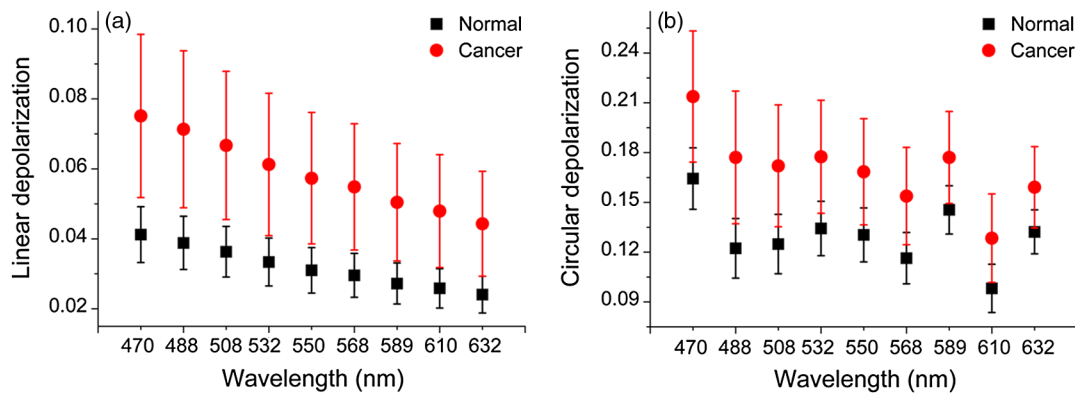
Fig. 5 (a) Linear depolarization and (b) circular depolarization of normal (■) and cancerous (●) gastric samples at nine different wavelengths ranging from 470 to 632 nm.

linear depolarization between normal and cancer samples appear to be smaller than circular depolarization, which suggests that linear depolarization likely differentiate between them more effectively than circular depolarization.

To quantitatively investigate the diagnostic values of these polarization parameters over the spectral range, linear discriminant analysis was performed to differentiate cancer samples from normal samples at all nine wavelengths.

Figure 6(a) shows that the classification using one single polarization parameter yields the decreasing overall accuracy in the order of retardance, depolarization, and diattenuation at

most wavelengths. The observation that diattenuation yields the lowest accuracy could be attributed to the highly overlapping error bars between cancer and normal samples as shown in Fig. 3(b). This could be related to the previous calculation that the ratio of the standard deviations in the diattenuation values of gastric samples to that of the optical components is only around two. Therefore, a significant portion of variance in the measured diattenuation values of gastric samples comes from the system thus being not reliable for classification. Figure 6(b) indicates that linear retardance always yields higher overall accuracy compared to circular retardance, which validates the
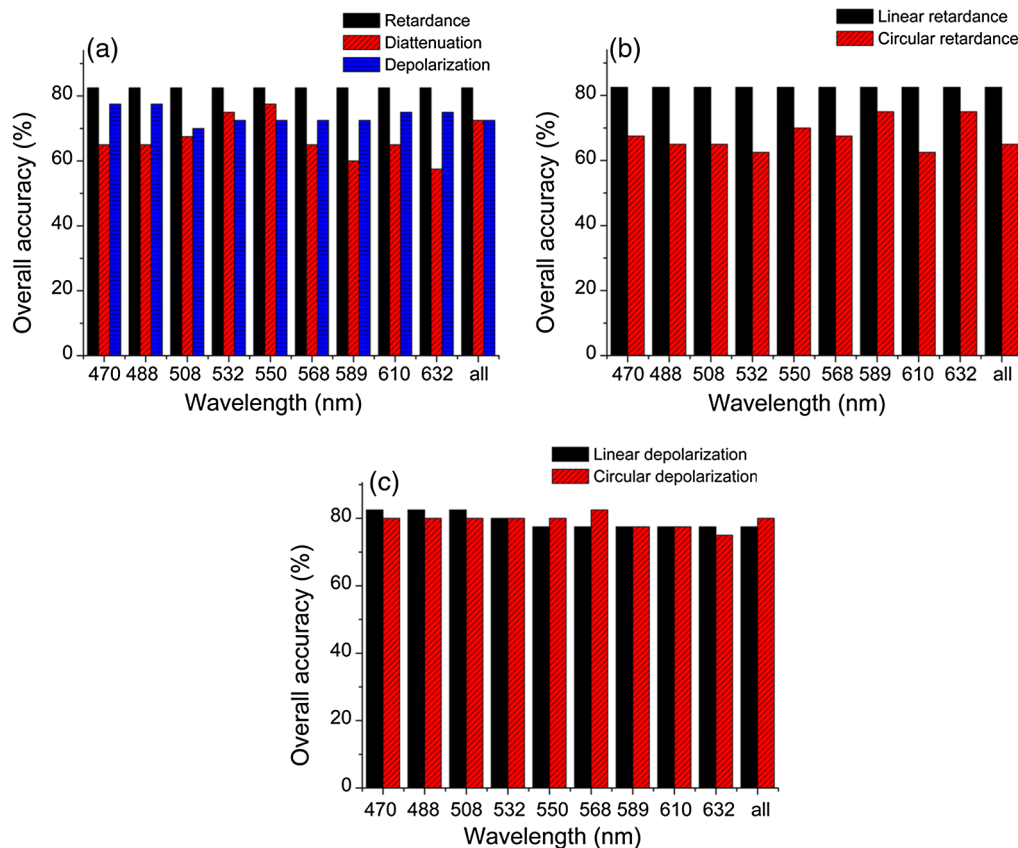

Fig. 6 LDA classification accuracy (overall accuracy) for (a) retardance, diattenuation, and depolarization, (b) linear and circular retardances, and (c) linear and circular depolarizations at nine different wavelengths ranging from 470 to 632 nm.

prediction made earlier according to Fig. 3. Figure 6(c) shows that linear depolarization yields slightly higher overall accuracy at some wavelengths but lower overall accuracy at other wavelengths compared to circular depolarization.

To find the optimal combination of polarization parameters for classification, a Wilcoxon rank sum test was performed at each wavelength for all parameters to decide which parameters should be used for combination. Table 1 presents the *p*-values calculated from the Wilcoxon test. With a significance level of 0.05, it was found that most parameters except diattenuation and circular retardance show significant differences between normal and cancerous gastric samples at all wavelengths, which agree well with the low classification accuracy of these two parameters shown in Fig. 6.

Then, all the possible combinations of these polarization parameters except diattenuation and circular retardance were used for classification based on the results of Wilcoxon rank sum tests. Table 2 shows the best combinations including a different number of polarization parameters at all wavelengths. It was found that the combination of linear depolarization (LD) and linear retardance (δ) shows the highest overall accuracy (95.00%) among all the possible combinations of two parameters. This combination also demonstrates considerable improvement in overall accuracy compared to that for either linear retardance (82.50%) or linear depolarization (77.50%) alone.

4 Discussion

In this study, we built a multispectral Mueller matrix imaging system, which was used to measure unstained gastric tissue sections from 470 to 632 nm. A full set of tissue polarization parameters was derived from measurements, which were then used to discriminate gastric cancer from normal samples in an attempt to investigate the individual roles of linear and circular polarization properties and the effect of wavelength choice on classification accuracy. Several interesting findings were made as discussed below.

Table 2 Accuracy of classification using the combination of two, three, four, and five parameters at all wavelengths.

Number of parameters	Best combination	Overall accuracy (%)	Sensitivity (%)	Specificity (%)
2	LD + δ	95.00	95.00	95.00
3	LD + δ + R	90.00	95.00	85.00
4	LD + δ + R + CD	90.00	90.00	90.00
5	LD + δ + R + CD + Δ	90.00	85.00	95.00

It is noted in Figs. 3(a) and 3(b) that error bars for the retardance and diattenuation of normal samples are slightly larger than those for cancer samples. The trend is the opposite for depolarization as shown in Fig. 3(c), for which the error bars for cancer samples are much larger. The higher variation in the retardance of normal samples could be possibly attributed to the higher variation in the types of tissue components, such as fibrous stroma and various glands, responsible for retardance.[2,11] When normal gastric tissues become malignant there are both architectural and cytological changes. The glands invade the mucosa and become disorganized, which then develop into cancers. In the process, the nucleocytoplasmic ratio increases and nuclei become vesicular and variable in size and shape. In addition, the tumor-associated stroma in cancer samples shows modification at both histological and molecular levels. The fibroblasts become "activated," which are termed as "cancer associated fibroblasts." Proliferation of endothelial cells and increased number of inflammatory cells may also be observed in the tumor-associated stroma. The above-mentioned stromal changes help to form a microenvironment that allows the growth of the tumor and increased angiogenesis and metastasis. This matches the previous reports[1,21] that the malignant changes in

Table 1 *P*-values obtained from Wilcoxon rank sum tests for polarization parameters at nine wavelengths for differentiation between normal and cancer samples.

	Polarization parameters						
λ (nm)	*R*	Dia	Δ	δ	φ	LD	CD
470	3.50E-06	0.0385	3.07 E-06	2.69 E-06	0.0154	3.07 E-06	4.68 E-05
488	4.54 E-06	**0.6359**	3.50 E-06	4.54 E-06	**0.2085**	4.54 E-06	7.58 E-06
508	5.87 E-06	0.0098	1.81 E-06	5.17 E-06	**0.1479**	5.17 E-06	2.92 E-05
532	5.17 E-06	0.0003	9.75 E-06	6.67 E-06	**0.0640**	1.25 E-05	3.71 E-05
550	3.50 E-06	**0.5428**	2.04 E-06	2.36 E-06	0.0207	5.87 E-06	9.28 E-05
568	5.17 E-06	0.0071	1.81 E-06	4.54 E-06	0.0315	5.17 E-06	4.68 E-05
589	2.69 E-06	**0.8817**	3.71 E-06	2.69 E-06	0.0020	5.17 E-06	1.79 E-04
610	5.17 E-06	**0.2085**	5.25 E-06	5.17 E-06	0.0294	6.67 E-06	2.75 E-04
632	3.07 E-06	0.0256	1.44 E-04	3.50 E-06	0.0179	7.58 E-06	2.00 E-04

Note: *R* – Retardance, Dia – Diattenuation, Δ– Depolarization, δ– Linear retardance, φ– Circular retardance, LD – Linear depolarization, CD – Circular depolarization. The entries with bold font indicate *p*-values larger than 0.05, which implies insignificant difference between normal and cancer samples at a significance level of 0.05.

the basal membrane include the alteration in the structures and ratios between various components, such as collagen and fibronectin, and that there are cross-linked fibrin accumulated in tumor fibrous stroma. This could be the major reason for larger retardance and linear retardance values in cancerous samples compared to normal samples. Typical H&E images of both stained normal and cancer gastric samples taken under 10× objective lens are shown in Fig. 7. It can be observed that gastric glands become more disorganized and there are more disorganized fibrous structures in the cancer samples compared to the normal one. Moreover, these components in normal samples are less consistent than that in cancerous samples due to the fact that normal samples obtained from biopsy procedures were much smaller than cancer samples obtained from surgery procedures. Thus, fewer measurements were thus performed for averaging from normal samples compared to cancer samples, which potentially resulted in larger error bars in the retardance of normal samples. As for the trend for depolarization, nuclei size and nuclei density, which are known to increase from normal samples to cancer samples as mentioned above, are less consistent in cancerous samples due to variance in the size of tumors for different patients,[22] which is also based on pathologist's observation and report from National University Hospital. This inconsistency should contribute to higher variances for cancerous samples in depolarization (Fig. 3), linear and circular depolarizations (Fig. 5) that are tightly related to nuclei size and nuclei density.[2,11] In addition, it could be observed from Fig. 5 that the values of circular depolarization are significantly higher than those of linear depolarization. This could be due to the fact that circularly polarized light was strongly affected by paraffin wax used to fix samples. The measurement of paraffin wax alone demonstrates significant circular depolarization for a wax layer of 4 μm (result not shown). However, we believe that the existence of wax does not affect our conclusion because the effect of wax was equally present in both normal and cancer samples. Besides, the higher retardance and depolarization in cancer could be partially attributed to stronger scattering resulting from enlarged nuclei and larger nuclei density.[11] The small mean values and large error bars of diattenuation and circular retardance were observed for gastric samples in this study, which may suggest that most tissue components in thin tissue sections are not strongly birefringent for circularly polarized light and not strongly diattenuating.

In Table 2, which shows the accuracy of classification using the combination of different parameters, it is interesting to observe that the overall accuracy does not improve as the number of parameters combined increases. Linear retardance and linear depolarization are included in all best combinations. This implies that these two parameters, which can be extracted from 3 × 3 Mueller matrix, are likely most important for clinical classification. Retardance is the third additional parameter in the best combination of three parameters while circular depolarization shows up in the best combination of four parameters. The derivation of both retardance and circular depolarization requires 4 × 4 Mueller matrix.

To investigate the effect of wavelength choice on classification accuracy, all the possible combinations of the nine wavelengths with the number of wavelengths ranging from 1 to 9 were evaluated for all the individual parameters (data not shown due to the large space required) except diattenuation and circular retardance that have been shown to be unable to effectively distinguish between normal and cancer samples according to Table 1. It was found that short wavelengths including 470 and 488 nm appear most frequently in the best combinations for depolarization and linear depolarization but the differences in classification accuracy between the optimal combination and other combinations are small. Moreover, all the combinations of wavelengths regardless of the number of wavelengths show nearly identical classification accuracy for retardance and linear retardance. Interestingly, it is also observed from Fig. 6 that the overall classification accuracy does not change significantly from one wavelength to another or to the combination of all wavelengths. This observation suggests that wavelength might not be a critical factor in terms of classification accuracy in this particular setup in which tissue samples were 4 μm in thickness only. It should be aware that this trend could change when tissue samples are thicker, in which case a reflection setup is required and the light path would be longer. A greater path length would result in larger retardance and diattenuation. The subsequent multiple scattering could increase depolarization. For a similar reason, the polarization properties at a shorter wavelength, at which case light scattering is usually stronger and light path is longer, may yield significantly different accuracy from those at a longer wavelength. Due to the scarcity of polarization properties of gastric tissue samples in the literature, we had to compare our findings with those for
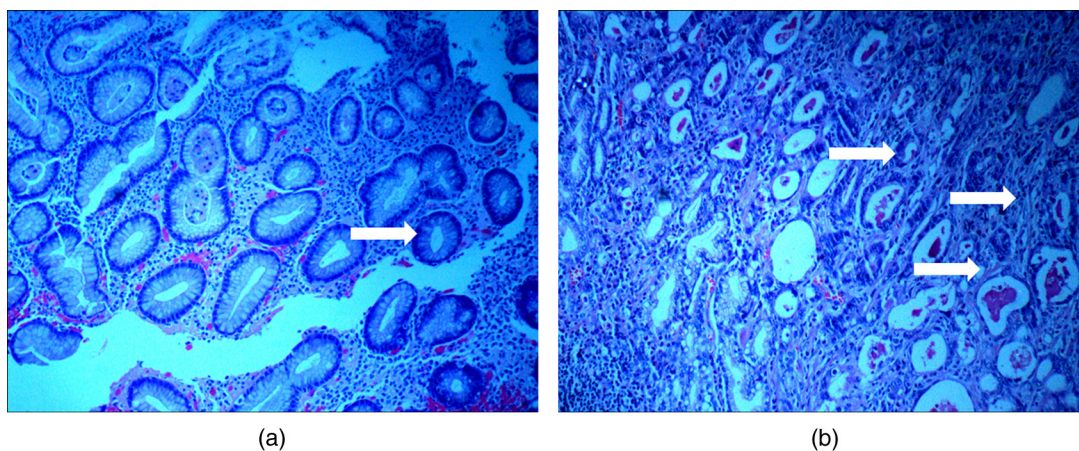

| (a) | (b) |

Fig. 7 H&E images for normal (a) and cancer (b) gastric samples under 10× objective lens. In the left image, the arrow points to a normal gastric gland. In the right image, the top arrow points to a malignant gland while the other two point to intervening disorganized fibrous stroma.

Table 3 Comparison in the polarization properties between the results of this study and those from the literature.

Polarization parameters	Gastric sample (this study, normal versus cancer)	Cervical sample (Normal versus precancer)[11]	Breast sample (Normal versus. cancer)[12]	Oral tissue (Normal versus cancer)[12]	Oral tissue (Normal versus precancer)[4]	Colon sample (Normal versus cancer)[23]
Retardance (R)	$R_n < R_c$	$R_n > R_p$	NA	NA	$R_n > R_p$	NA
Diattenuation (Dia)	$\text{Dia}_n \approx \text{Dia}_c$	NA	$\text{Dia}_n < \text{Dia}_c$	$\text{Dia}_n > \text{Dia}_c$	NA	NA
Depolarization (Δ)	$\Delta_n < \Delta_c$	$\Delta_n < \Delta_p$	NA	NA	$\Delta_n > \Delta_p$	$\Delta_n > \Delta_c$
Linear retardance (δ)	$\delta_n < \delta_c$	NA	$\delta_n < \delta_c$	$\delta_n > \delta_c$	NA	NA
Circular retardance (φ)	$\varphi_n \approx \varphi_c$	NA	NA	NA	NA	NA
Linear depolarization (LD)	$\text{LD}_n < \text{LD}_c$	NA	$\text{LD}_n > \text{LD}_c$	$\text{LD}_n < \text{LD}_c$	NA	NA
Circular depolarization (CD)	$\text{CD}_n < \text{CD}_c$	NA	NA	NA	NA	NA

Note: the subscripts with "n", "c", and "p" indicate normal, cancer, and precancer samples. "NA" infers that relevant data are not available.

other types of tissue samples from the literature as shown in Table 3. It is observed that our results for gastric samples are consistent with those for cervical or breast samples in depolarization and linear retardance but disagree with those for oral and colon samples in retardance, diattenuation, depolarization, and linear retardance. This is possibly related to the differences in the polarimetry imaging configuration and the biological structure of tissue samples from one study to another. For example, the measured polarimetry signal could be sensitive to different biological structures in each type of tissue samples if the configuration is arbitrarily sensitive to a fixed depth, as the biological structure can vary with the tissue type. This suggests the importance of studying the polarization properties of individual cell types, such as those in foveolar, pyloric, and oxyntic glands, rather than normal or cancer samples in general. Compared to other tissue studies, this study yields a comprehensive collection of polarization parameters, which will provide a reference for subsequent studies in the future.

5 Conclusion

A multispectral 4×4 Mueller matrix imaging system was used to investigate *ex vivo* gastric tissue section samples that were not stained. There were significant differences in most polarization parameters, including retardance, depolarization, linear retardance, linear depolarization, and circular depolarization, between normal and cancer gastric samples. The combination of linear depolarization and linear retardance yields the highest accuracy in sample classification. When the depolarization of linearly polarized light due to scattering is independent of the orientation angle of the incident linear polarization vector, the derivation of linear polarization properties will require only 3×3 Mueller matrix, which would significantly reduce the complexity of the polarimetry imaging system. When additional parameters are needed to complement the two linear polarization parameters, retardance, circular depolarization, and depolarization can be included in classification in the order of preference. However, these additional parameters would require the measurement of 4×4 Mueller matrix. In addition, it appears that wavelength is not a critical factor in terms of classification accuracy for thin tissue sections in this study.

References

1. A. I. Baba and C. Câtoi, "Tumor cell morphology," Chapter 3 in *Comparative Oncology*, A. I. Baba and C. Catoi, Eds., pp. 119–125, The Publishing House of the Romanian Academy, Bucharest (2007).
2. N. Ghosh and I. A. Vitkin, "Tissue polarimetry: concepts, challenges, applications, and outlook," *J. Biomed. Opt.* **16**(11), 110801 (2011).
3. R. A. Chipman, "Polarimetry," Chapter 22 in *Handbook of Optics*, 2nd ed., M. Bass, Ed., Vol. 2, pp. 22.1–22.37, McGraw-Hill, New York (1994).
4. J. R. Chung et al., "Use of polar decomposition for the diagnosis of oral precancer," *Appl. Opt.* **46**(15), 3038–3045 (2007).
5. M. K. Swami et al., "Polar decomposition of 3x3 Mueller matrix: a tool for quantitative tissue polarimetry," *Opt. Express* **14**(20), 9324–9337 (2006).
6. Q. Liu et al., "Development of a synchronous fluorescence imaging system and data analysis methods," *Opt. Express* **15**(20), 12583–12594 (2007).
7. Q. Liu and T. Vo-Dinh, "Spectral filtering modulation method for estimation of hemoglobin concentration and oxygenation based on a single fluorescence emission spectrum in tissue phantoms," *Med. Phys.* **36**(10), 4819–4829 (2009).
8. Q. Liu et al., "Compact point-detection fluorescence spectroscopy system for quantifying intrinsic fluorescence redox ratio in brain cancer diagnostics," *J. Biomed. Opt.* **16**(3), 037004 (2011).
9. M. H. Smith et al., "Mueller matrix imaging polarimetry in dermatology," *Proc. SPIE* **3911**, 210–216 (2000).
10. A. M. Baldwin et al., "Mueller matrix imaging for cancer detection," in *Proc. 25th Annual International Conference of the IEEE Engineering in Medicine and Biology Society*, Vols 1–4: A New Beginning for Human Health, pp. 1027–1030, Institute of Electrical and Electronics Engineers, Mexico (2003).
11. P. Shukla and A. Pradhan, "Mueller decomposition images for cervical tissue: Potential for discriminating normal and dysplastic states," *Opt. Express* **17**(3), 1600–1609 (2009).
12. S. Manhas et al., "Polarized diffuse reflectance measurements on cancerous and noncancerous tissues," *J. Biophotonics* **2**(10), 581–587 (2009).
13. A. Pierangelo et al., "Ex-vivo characterization of human colon cancer by Mueller polarimetric imaging," *Opt. Express* **19**(2), 1582–1593 (2011).

14. B. Laude-Boulesteix et al., "Mueller polarimetric imaging system with liquid crystals," *Appl. Opt.* **43**(14), 2824–2832 (2004).
15. J. Soni et al., "Quantitative fluorescence and elastic scattering tissue polarimetry using an Eigenvalue calibrated spectroscopic Mueller matrix system," *Opt. Express* **21**(13), 15475–15489 (2013).
16. S. Y. Lu and R. A. Chipman, "Interpretation of Mueller matrices based on polar decomposition," *J. Opt. Soc. Am. A* **13**(5), 1106–1113 (1996).
17. N. Ghosh, M. F. G. Wood, and I. A. Vitkin, "Mueller matrix decomposition for extraction of individual polarization parameters from complex turbid media exhibiting multiple scattering, optical activity, and linear birefringence," *J. Biomed. Opt.* **13**(4), 044036 (2008).
18. Y. H. Guo et al., "A study on forward scattering Mueller matrix decomposition in anisotropic medium," *Opt. Express* **21**(15), 18361–18370 (2013).
19. I. C. Buscemi, S. Guyot, and J. Lemoine, "New imaging technique using Degree Of Polarization for the study of polarimetric properties for non-invasive biomedical diagnostic," *Proc. SPIE* **8427**, 842706 (2012).
20. X. Li and G. Yao, "Mueller matrix decomposition of diffuse reflectance imaging in skeletal muscle," *Appl. Opt.* **48**(14), 2625–2631 (2009).
21. L. F. Brown et al., "Fibrinogen influx and accumulation of cross-linked fibrin in healing wounds and in tumor stroma," *Am. J. Pathol.* **130**(3), 455–465 (1988).
22. G. Guzman and G. Chejfec, "Tumors of the digestive system," in *Cancer Grading Manual*, I. Damjanov and F. Fan, Eds., 1st ed., pp. 35–46, Springer, New York (2007).
23. M.-R. Antonelli et al., "Mueller matrix imaging of human colon tissue for cancer diagnostics: how Monte Carlo modeling can help in the interpretation of experimental data," *Opt. Express* **18**(10), 1094–4087 (2010).

Wenfeng Wang received his BS degree in science in 2011 from Jilin University, Ji Lin, China. He is currently a PhD student in Quan Liu's lab. His current research interest is to develop fast polarimetry imaging system for early cancer detection.

Lee Guan Lim received his MBBS degree from National University of Singapore, and the MRCP degree from Royal College of Physicians, United Kingdom. He is currently a consultant, postgraduate training director, and program director of the ACGME-I Gastroenterology Fellowship Program in National University Health System, Singapore. He has published several academic papers in peer-reviewed journals and written multiple book chapters.

Supriya Srivastava is a pathologist at the Cancer Science Institute, National University of Singapore. She received her postgraduate medical degree (MD) at King George's Medical University in 2007. Her areas of research include identifying biomarkers in patients at high risk of gastric cancer, prognostic biomarkers in hepatocellular carcinoma, and cervical carcinoma.

Jimmy So Bok Yan is an associate professor of surgery at National University of Singapore and senior consultant general and upper gastrointestinal surgeon at National University Hospital, Singapore. He graduated from the Chinese University of Hong Kong and then received his surgical training at National University Hospital, Singapore. His specialty is in general surgery and his special interests are in upper gastrointestinal, bariatric, minimally invasive, and hernia surgeries.

Asim Shabbir received his MBBS degree from University of Punjab, Lahore, Pakistan. He is a consultant within the division of general surgery (upper gastrointestinal surgery) at the National University Hospital, Singapore. He completed his basic and advanced surgical training at National University Hospital, Singapore.

Quan Liu received his PhD degree in biomedical engineering from the University of Wisconsin, Madison. He is currently an assistant professor in the school of chemical and biomedical engineering at Nanyang Technological University in Singapore. His research interest is focused on optical imaging and spectroscopy for medical diagnostics. He has published around 30 journal papers and held nine US patents/applications. He is a senior SPIE member and a regular OSA member.